Nanoscale

Accepted Manuscript

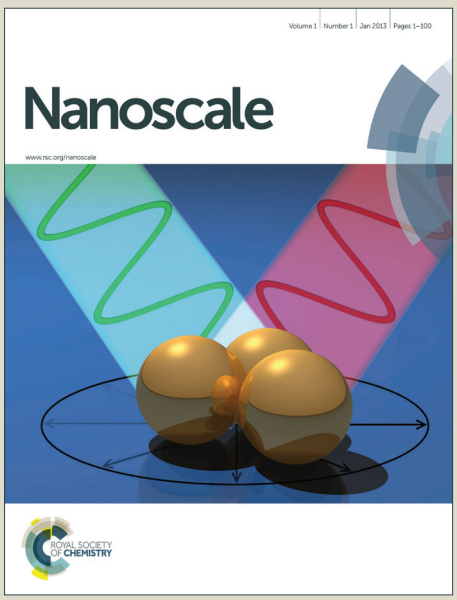

This is an *Accepted Manuscript*, which has been through the Royal Society of Chemistry peer review process and has been accepted for publication.

Accepted Manuscripts are published online shortly after acceptance, before technical editing, formatting and proof reading. Using this free service, authors can make their results available to the community, in citable form, before we publish the edited article. We will replace this *Accepted Manuscript* with the edited and formatted *Advance Article* as soon as it is available.

You can find more information about *Accepted Manuscripts* in the Information for Authors.

Please note that technical editing may introduce minor changes to the text and/or graphics, which may alter content. The journal's standard Terms & Conditions and the Ethical guidelines still apply. In no event shall the Royal Society of Chemistry be held responsible for any errors or omissions in this *Accepted Manuscript* or any consequences arising from the use of any information it contains.

ROYAL SOCIETY OF CHEMISTRY

www.rsc.org/nanoscale

Please do not adjust margins

Nanoscale

PAPER

Fully Solution-Processed Transparent Electrodes Based on Silver Nanowire Composites for Perovskite Solar Cells

Received 00th January 20xx,
Accepted 00th January 20xx

DOI: 10.1039/x0xx00000x

www.rsc.org/

Areum Kim,[a] Hongseuk Lee,[a] Hyeok-Chan Kwon,[a] Hyun Suk Jung,[b] Nam-Gyu Park,[c] Sunho Jeong,[d] and Jooho Moon[a,*]

We report all-solution-processed transparent conductive electrodes based on Ag nanowire (AgNW)-embedded metal oxide composite films for application in organometal halide perovskite solar cells. To address the thermal instability of Ag nanowires, we used combustive sol-gel derived thin films to construct ZnO/ITO/AgNW/ITO composite structures. The resulting composite configuration effectively prevented the AgNWs from undergoing undesirable side-reactions with halogen ions present in the perovskite precursor solutions that significantly deteriorate the optoelectrical properties of Ag nanowires in transparent conductive films. AgNW-based composite electrodes had a transmittance of ~80% at 550 nm and sheet resistance of 18 Ω sq^{-1}. Perovskite solar cells fabricated using a fully-solution-processed transparent conductive electrode, Au/spiro-OMeTAD/$CH_3NH_3PbI_3$+m-Al_2O_3/ ZnO/ITO/AgNW/ITO, exhibited a power conversion efficiency of 8.44% (comparable to that of the FTO/glass-based counterpart at 10.81%) and were stable for 30 days in ambient air. Our results demonstrate the feasibility of using AgNWs as a transparent bottom electrode in perovskite solar cells produced by a fully-printable process.

Introduction

Low-cost, high efficiency photovoltaics have been persistently pursued over the past decade to realize renewable solar energy conversion. Organometal halide perovskites, most commonly $CH_3NH_3PbI_3$ or close variants, have been highlighted as outstanding earth-abundant photovoltaic materials because of their high efficiencies and low-cost processing potentials.[1-5] The highest power conversion efficiency (PCE) reported thus far for perovskite solar cells is 20.1%. In terms of the fabrication process, well-crystallized dense perovskite absorber films are easy to fabricate via a solution process, allowing for relative simple and economical production of solar cells. However, a high vacuum process is still used for electrode deposition in perovskite solar cells. Counter-electrodes such as Au or Ag are usually prepared by thermal evaporation, whereas sputtered fluorine doped tin oxide (FTO) or indium tin oxide (ITO) films are commonly used as transparent electrodes. Because vacuum evaporation and sputtering processes consume large amounts of energy and increase manufacturing costs, an alternative method to replace the vacuum method is required to achieve the ultimate goal of all-solution-processed perovskite solar cells for inexpensive, high-efficiency photovoltaic systems.

Liu *et al*. recently reported that a low-cost carbon counter electrode could substitute for the vacuum-deposited Au electrode.[6-7] Perovskite solar cells with printed carbon electrodes showed reasonable performance and stability; however, the FTO electrode was still sputtered on the glass substrate. For fully printable perovskite solar cell, the transparent electrode should also be solution-processable. To achieve solution-processed transparent electrodes, high conductivity and stability are required, because a high performance transparent electrode is needed in a solar cell system to allow sufficient sunlight to be transmitted to the absorber layer, while charge carriers need to be effectively collected to minimize current loss.

Silver nanowire (AgNW) networks are attractive candidates for alternative transparent conductive electrodes. A transparent film of AgNW networks could be deposited by a simple solution-based method such as bar coating, spin coating, or spray deposition, with the expectation that the resulting AgNW percolation networks would act as a high conductivity electron pathway. Several studies have reported using AgNWs as transparent electrodes in a wide variety of solar cells such as organic photovoltaic cells, dye-sensitized solar cells, and thin film solar cells.[8-14] This implies that AgNWs

[a] Department of Materials Science and Engineering, Yonsei University, Seoul 120-749, Republic of Korea. Email: jmoon@yonsei.ac.kr
[b] School of Advanced Materials Science & Engineering, Sungkyunkwan University, Suwon 440-746, Republic of Korea
[c] School of Chemical Engineering and Department of Energy Science, Sungkyunkwan University, Suwon 440–746, Republic of Korea
[d] Division of Advanced Materials, Korea Research Institute of Chemical Technology (KRICT),Daejeon 305-600, Republic of Korea

† Electronic Supplementary Information (ESI) available: See DOI: 10.1039/x0xx00000x

Nanoscale Accepted Manuscript

Please do not adjust margins

are potential transparent electrodes for perovskite solar cells. However, there are critical hurdles to be resolved prior to the application of AgNWs to perovskite solar cell. When AgNWs come into contact with the perovskite precursor solution containing halogen ions, degradation of the AgNWs occurs due to reaction between Ag and halogen ions.[15] In previous reports, AgNWs have therefore simply been utilized as the top electrode underlying the hole transport layer to avoid damage to the AgNWs during the precursor coating process.[1,16] Recently, Han *et al.* reported using a AgNW-based electrode on the bottom layer together with an ~100 nm-thick pulsed laser-deposited overcoat layer of ZnO:F. Although the power conversion efficiency (PCE) of the resulting solar cell was relatively low (~ 3.29%), the possibility that AgNWs could be used in perovskite solar cells was suggested.[17] However, no all-solution-processed transparent electrodes for fully-printable perovskite solar cells have been reported to date.

Here, we report the development of silver nanowire-based composite electrodes as effective, solution-processable electrodes for perovskite solar cells. To apply AgNWs as a bottom layer to construct perovskite solar cells, chemical stability is of critical importance. A blocking layer is necessary not only to prevent contact between halogen ions and Ag during precursor coating and annealing, but also to prevent the silver from migrating into the perovskite absorber. This blocking layer should also effectively collect charge carriers. We synthesized sol-gel derived dense conductive ITO and ZnO films. These layers should form at a temperature low enough not to thermally impair the AgNWs, which happens at ~225℃.[13] For low temperature annealing of ITO and ZnO films (below 250℃), we utilized a redox-based combustion synthetic approach.[14,18] The resulting composite electrode had the multi-stacking structure of ZnO/ITO/AgNW/ITO and exhibited a transmittance of 79.5% at 550 nm with a sheet resistance of 18 Ω/sq. The ZnO layer functioned as a hole blocking layer on the composite electrode. A perovskite solar cell fabricated using the AgNW composite electrode showed reasonable current density-voltage (*J-V*) performance with a PCE of 8.44% compared to the PCE of 10.98% obtained using commercial FTO substrate. These results clearly demonstrate the feasibility of using AgNWs as all-solution-processed transparent electrodes in perovskite solar cells.

Experimental

Preparation of ZnO and ITO sol–gel precursor solution

For the ZnO solution, zinc nitrate hexahydrate ($Zn(NO_3)_2{\cdot}6H_2O$, 99%, Alfa Aesar, Ward Hill, MA, USA) and zinc acetylacetonate ($Zn(C_2O_5H_5)_2$, 99.995%, Sigma Aldrich) were dissolved in 2-methoxyethanol (anhydrous, 99.8%, Sigma Aldrich) at a molar ratio of 1:1. The total concentration of the metal precursors was 0.15 M. Precursor solutions were aged for 18 h prior to spin coating. ITO sol-gel solution was also prepared by using a previously reported method with slight modification.[18] Indium(III) nitrate hydrate ($In(NO_3)_3{\cdot}xH_2O$, 99.999%, Sigma Aldrich) or tin(II) chloride ($SnCl_2$, 99.99%, Sigma Aldrich) was dissolved in 2-methoxyethanol with NH_4NO_3, followed by addition of acetlyacetone (≥99%, Sigma Aldrich). Total concentration of metal precursors was 0.8 M for the bottom ITO layer and 0.25 M for the overcoat ITO on the AgNW film. After complete dissolution, NH_3(aq) was added and the solution was aged for 12 h. For the ITO solution, In:Sn at a molar ratio of 9:1 was made by mixing the two component solutions and stirring for 1 h before film casting.

Composite electrode fabrication

The ITO/AgNW/ITO multilayer was prepared by successive spin coating. Soda-lime glasses were cleaned sequentially using acetone, distilled water, and ethanol in an ultrasonic bath, and treated in an O_2 plasma cleaner for 10 min. The ITO bottom layer was deposited via spin coating at 2000 rpm for 30 s, followed by drying at 150°C for 90 s and 200°C for 10 min. Post annealing was performed in a H_2/Ar (5/95) atmosphere at 500°C for 30 min. Then, the AgNW film was deposited on the bottom ITO layer by spin coating, and the AgNW density was controlled by the rotation speed used for AgNW ink (AgNW-25, Seashell Technology, CA, USA). The AgNWs are dispersed in H_2O, and the diameter and length of AgNW were measured to be around 40 nm and over 20 μm, respectively. After drying AgNW film at 150°C for 90 s, the ITO overcoat layer was deposited by spin coating at 2500 rpm for 30 s. It was then dried at 200°C for 10 min and post-annealed at 200°C for 30 min in a H_2/Ar (5/95) atmosphere. Oxygen plasma cleaning was performed between successive coating processes using plasma cleaner (PDC-002, Harrick Plasma, New York, USA) for 5 min at a medium power. The surface cleaning procedure between subsequent multi-coating processes is quite important to enhance the quality of resulting composite electrodes by removing organic contaminants as well as to obtain the sufficient surface-wetting behavior. UVO cleaner is not recommended for the case of AgNW-based films, as UV light, penetrated through metal oxide overcoat-layers, can cause the surface oxidation of AgNWs.

Optical, structural, and electrical characterization

Optical transmittances of the transparent composite electrodes were measured at room temperature using a UV-vis spectrophotometer (V-530, Jasco, Oklahoma City, OK, USA) including glass substrates. All recorded transmittance spectra represented a regular transmittance, and was measured after calibration in air. The surface and cross section of the composite electrodes were analyzed by field emission scanning electron microscopy (FE-SEM, JSM-7001F, JEOL Ltd., Tokyo, Japan). The sheet resistances of the ITO/AgNW/ITO samples were measured by a 4-point probe system (RS8, BEGA Technologies, Seoul, Korea) as a function of AgNW density as expressed by the covered area ratio (CAR). The resistance reported herein is the average of five measurements. Film crystallinity was determined using an X-ray diffractometer (Rigaku Miniflex 600, The Woodlands, TX, USA). To monitor resistance changes, resistance values were measured using a multi-meter (Fluke 17B+, Everett, WA, USA). Samples were

Nanoscale Accepted Manuscript

This journal is © The Royal Society of Chemistry 20xx

prepared by partial deposition of perovskite precursor solution on the AgNW and ZnO/AgNW films using PI tape masking of both sides of the substrate for electrical contacts.

Synthesis of CH_3NH_3I

Methylamine (27.86 ml, 40% in methanol, TCI) and hydroiodic acid (30 ml, 57 wt% in water, Sigma-Aldrich) were mixed at 0°C and stirred for 2 h. The precipitate was recovered by evaporation at 50°C for 1 h. The product was washed with diethyl ether three times and finally dried at 60°C in a vacuum oven for 24 h.

Fabrication of perovskite solar cells

A ZnO blocking layer was spin-coated at 2500 rpm for 30 s on the ITO/AgNW/ITO composite electrode using 0.15 M ZnO sol-gel solution. After drying at 200°C for 90 s, coating and drying were repeated four more times to obtain a film thickness of about 50 nm. The film was annealed at 200°C for 10 min. For the mesoporous Al_2O_3 film, an Al_2O_3 nanoparticle dispersion (20 wt% in 2-propanol, Sigma Aldrich) was diluted to 3.5 wt% with 2-propanol, and spin coated at 2500 rpm for 60 s. The film was dried at 200°C for 30 min. The $CH_3NH_3PbI_3$ absorber layer was produced via a two-step spin coating procedure. PbI_2 solution (1 M) was prepared by dissolving 463 mg PbI_2 (99%, Sigma Aldrich) in 1 ml N,N-dimethylformamide (DMF, 99.8%, Sigma Aldrich) under stirring at 70°C. PbI_2 solution was spin-coated on the mesoporous Al_2O_3 film at 6000 rpm for 5 s, and after spinning, the film was dried at 70°C for 30 min. After cooling to room temperature, PbI_2-coated substrates were immersed in 0.063 M $CH_3NH_3PbI_3$ solution (10 mg ml^{-1} in 2-propanol, 99%, Sigma Aldrich) for 20 min, and annealed at 70°C for 30 min. A volume of 40 µl of 2,2′,7,7′-tetrakis(N,N-di-p-methoxyphenylamine)-9,9-spirobifluorene (spiro-MeOTAD, Borun Chemical, Ningbo, China) solution was spin-coated on the $CH_3NH_3PbI_3$ perovskite layer at 3000 rpm for 30 s. Spiro-OMeTAD solution was prepared by dissolving 72 mg of spiro-OMeTAD in 1 ml of chlorobenzene, to which 28.8 µl of 4-tert-butyl pyridine and 14.4 µl of lithium bis (trifluoromethanesulfonyl)imide (Li-TFSI) solution (520 mg LI-TSFI in 1 ml acetonitrile, Sigma Aldrich, 99.8%) were added. Perovskite and spiro-OMeTAD layers were fabricated in a glove box filled with dry mixed gas (O_2 : N_2 = 21% : 79%). Finally, 70 nm of gold was thermally evaporated on the spiro-OMeTAD-coated film.

Characterization of photovoltaic properties

Solar cells were characterized by measuring photocurrent density-voltage (*J–V*) curves and external quantum efficiency (EQE). The photovoltaic performance in terms of *J–V* characteristics of the devices was determined using a solar simulator (Sol3A Class AAA, Oriel Instruments, Stratford, CT, USA) and a Keithley 2400 source measurement unit (Keithley Instruments Inc., Cleveland, OH, USA) under air mass (AM) 1.5 and 1 sun (100 mW cm^{-2}) conditions. The 1 sun intensity level was calibrated using a standard Si reference cell certified by the Newport Corporation. All devices were measured in a light-tight sample holder, and the active area (0.06 cm^2) was determined by an aperture mask. PCE values were calculated from the measured J_{SC}, V_{OC}, and FF values by the formula PCE = FF x V_{OC} x J_{SC} / *P*s, where *P*s is the input solar irradiance (mW cm^{-2}). The FF term was defined as FF = J_m V_m / $J_{SC}V_{OC}$, where J_m and V_m are the maximum current and voltage values, respectively. EQE was obtained by a quantum efficiency measurement system (QEX10, PV Measurements, Inc.).

Results and discussion

Silver can be corroded by contacting with halogen ions due to formation of silver halide. Thus, AgNW film has not been applied to perovskite solar cells in contrast to other solar cell types, because perovskite absorbers, represented by $CH_3NH_3PbI_3$, contain halogen ions. Indeed, we observed the formation of an AgI phase by X-ray diffraction (XRD) when AgNWs were exposed to a precursor solution of PbI_2 and CH_3NH_3I. Because the main peak positions of AgI coincided with those of the perovskite phase (see Fig. S1†, Electronic Supplementary Information (ESI)), we identified the AgI phase by dividing the fabrication steps into PbI_2 coating (followed by drying) and dipping in CH_3NH_3I solution (followed by drying), as the diffraction peaks of PbI_2 and CH_3NH_3I phases did not overlap with the main peaks of AgI. In Fig. 1, AgI peaks (●) were clearly distinguishable from CH_3NH_3I (■), PbI_2 (▼), or AgNW (▲) peaks for 24 h aged samples. This result suggested that the AgI phase formed due to contact between AgNWs and iodine ions and that this phase formation was time-dependent. This reaction not only degrades the AgNWs, but also has an adverse effect on perovskite phase formation. Therefore, preventing this undesirable reaction is necessary when using AgNWs as a bottom electrode.

A barrier layer between the AgNWs and perovskite would prevent the migration of halogen ions into AgNWs. Standridge *et al.* reported that an atomic layer deposited (ALD) TiO_2 layer protected silver nanoparticles from corrosive I^-/I_3^- conditions,[19]

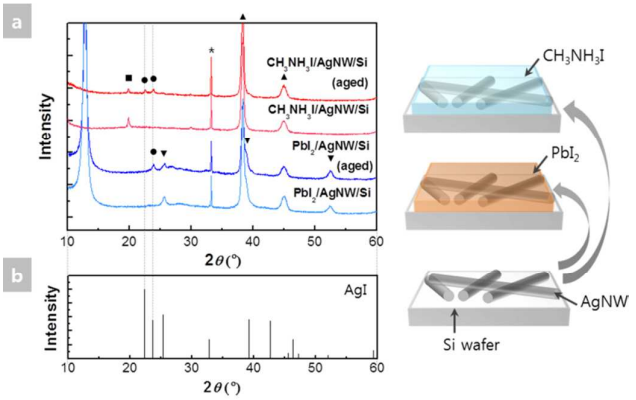

Fig. 1 (a) XRD spectra of PbI_2/AgNW/Si and $CH_3NH_3PbI_3$/AgNW/Si. Aged samples indicate that measurements were performed after 24 h of aging (AgI = ●, CH_3NH_3I = ■, PbI_2 = ▼, Ag = ▲, Si substrate = *). (b) Diffraction patterns of AgI power are highlighted by sticks (JCPDS 01-078-1614).

Nanoscale Accepted Manuscript

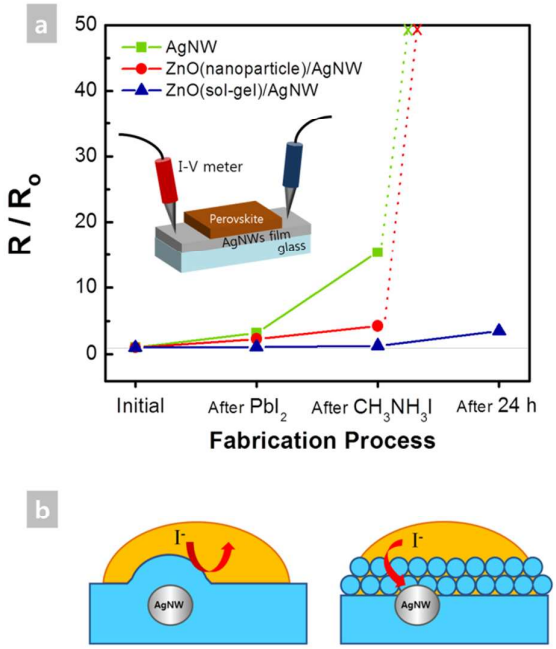

Fig. 2 (a) Resistance changes of AgNW film and ZnO/AgNW film during sequential perovskite deposition. After 24 h of aging, resistances were re-measured. (b) Schematics showing cross-sections of composite electrodes when perovskite precursor solution containing iodine ions was coated on either the AgNW-sol gel-derived dense composite electrode or AgNW-nanoparticulate porous composite electrode.

whereas Han *et al*. utilized a pulsed laser deposited (PLD) ZnO:F layer on AgNW film to protect the film.[17] These previous studies clearly demonstrated that metal oxides can protect AgNWs in a halogen environment; however, the films reported in the previous study were produced by vacuum processes. We focused on using solution-processable metal oxide film as a protective layer. The annealing temperature to create solution-processed metal oxide layer on top of AgNWs should be lower than 250°C to avoid thermal damage to AgNWs, as they are vulnerable to melting.[13] Two different types of ZnO films were prepared from either a nanoparticle dispersion or combustion sol-gel solution for low temperature annealing. Both ZnO layers had a thickness of ~50 nm. Resistance changes were monitored during perovskite solution coating to determine whether the barrier was capable of protecting AgNWs from adverse reactions. As shown in Fig. 2a, the resistance of bare AgNWs film increased sharply after deposition of the perovskite film. Although apparent AgI peaks were not observed immediately after PbI_2 coating (Fig. 1), the resistance of AgNWs film increased instantly. This implied that the amount of AgI phase that formed after PbI_2 deposition may have been insufficient to provide significant X-ray diffraction patterns, but that the AgNWs started to degrade upon exposure to the perovskite precursor solution, as observed by the increase in resistance. Application of a ZnO overlayer to the AgNW film suppressed resistance changes regardless of film type; in the case of the sol-gel based ZnO/AgNW film, the resistance after $CH_3NH_3PbI_3$ precursor deposition was almost the same as the initial resistance, whereas resistance increased by a factor of 4 for the nanoparticulate ZnO/AgNW film. After aging for 24 h, the resistances of the AgNW and nanoparticulate ZnO/AgNW films were not measured because the films lost their conductivity; however, the sol-gel based ZnO/AgNW film maintained its conductivity and showed slightly increased sheet resistance. The difference in protective characteristics of the two types of ZnO films can be explained in terms of their microstructures. Nanoparticle-based film annealed at 200°C had a porous structure, whereas the sol-gel based film had a relatively dense structure, indicating an amorphous state (Fig. 2b and Fig. 3a,b). Iodine ions likely penetrated through the porous nanoparticulate film, and reacted with AgNWs. Therefore, we selected the sol-gel approach to fabricate a solution-processed protection layer for AgNW film.

The transparent composite electrode for perovskite solar cells demonstrated here consisted of indium tin oxide (ITO) and AgNWs. Based on our previous studies of AgNW composite electrodes,[13,14] we used a sandwich-like structure (metal oxide/AgNW/metal oxide) due to its excellent mechanical stability and charge collection efficiency. The conductivity of the metal oxide matrix is important to enhance the overall conductivity of the composite structure. Therefore, we used ITO as a conductive matrix in which to embed the AgNWs, as ITO has the highest conductivity among solution-processable metal oxides. AgNW film was deposited from a AgNW dispersion, and ITO film was fabricated using a combustion sol-gel method. The combustion sol-gel derived ITO film had a dense cross-sectional structure, as shown in Fig. S2†, ESI. Although the crystallinity of the ITO film increased with an increase in annealing temperature, the films on the AgNWs had to be annealed below 250°C so as not to damage the AgNWs, therefore an amorphous phase was present as determined by XRD analysis (Fig. S3a†, ESI). The combustion reaction facilitated an exothermic reaction around ~190°C, which assisted film formation by annealing, even at 200°C (Fig. S3b†, ESI). The conductivity of ITO film was dependent on the annealing temperature, as shown in Table S1†, ESI.

The AgNW composite electrode was fabricated through a successive spin-coating process, as shown in Fig. 4a. ITO bottom layer was deposited on the glass substrate and after

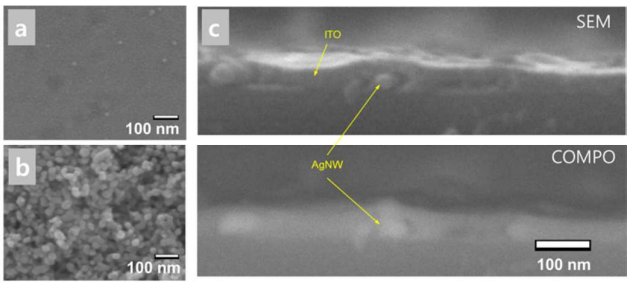

Fig. 3 The FE-SEM images of (a) amorphous sol-gel ITO film and (b) ITO nanoparticulate film. (c) Cross-sectional FE-SEM images of AgNWs over-coated by using 0.4M ITO sol-gel solution.

Nanoscale Accepted Manuscript

This journal is © The Royal Society of Chemistry 20xx

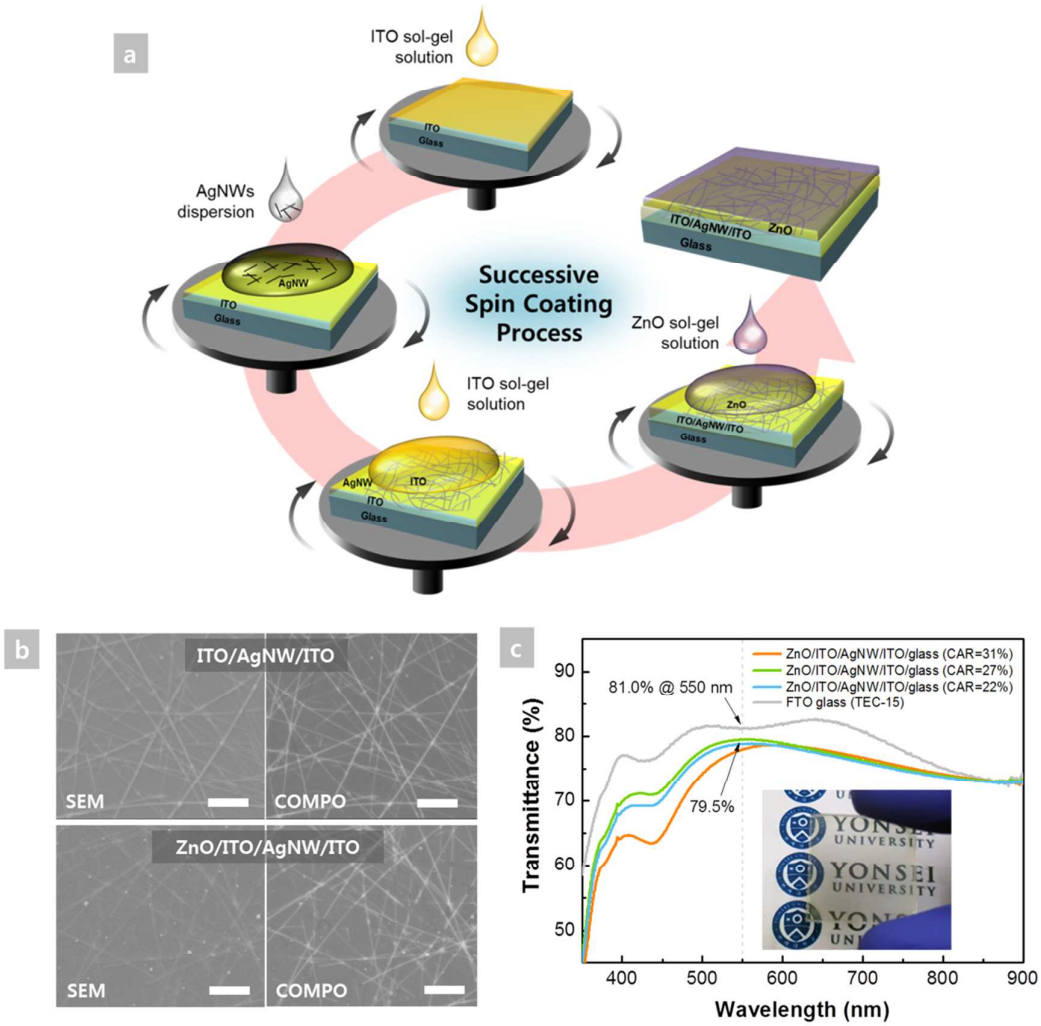

Fig. 4 (a) Schematics illustrating the successive spin coating processes used to fabricate the ZnO/ITO/AgNW/ITO composite structure. (b) FE-SEM images of composite electrodes in secondary electron (SE) mode and back scattered electron (BSE) COMPO mode. (c) Optical transmittance spectra of the composite electrodes on glass substrate as a function of AgNW density as well as FTO glass substrate. The inset is a photograph of the ITO/AgNW/ITO composite (CAR=27%) on glass substrate

annealing of the ITO film, AgNW film was deposited on the ITO film. The concentration of AgNWs was controlled by the spin coating speed, and their areal density was quantitatively evaluated in terms of *covered area ratio* (CAR) with the aid of image analysis [13]; detailed analysis processes are shown in Fig. S4†, ESI. The ITO top layer on the AgNWs was also deposited using spin coating, and this layer functioned both as a conductive matrix in which the AgNWs were tightly embedded and as a protective layer against halogen ion penetration into the AgNW film. We determined the concentration of ITO sol-gel solution as 0.25M to overcoat AgNWs by forming thin, conformal coating layer as shown in Fig. 3c. The thin ITO overcoat-layer cannot form a conformal film on top of AgNWs; it was verified by observing the thermal degradation of AgNWs covered with ITO sol-gel solutions with different concentrations (Fig. S5). The conformal metal oxide overcoat-layer can protect effectively AgNWs from a thermal damage. On the other hand, the thick ITO layer is not desirable due to the increase in sheet resistance. The sol-gel based ITO films require a post-treatment under a reduction atmosphere at high temperatures around 450-550 ^{o}C to achieve a low sheet resistance. However, in the case of top ITO layer, the post-treatment at high temperatures above 250 ^{o}C is not available due to thermal damages on AgNWs, which results in the relatively high resistivity of top ITO layer. The sheet resistances were evaluated as shown in Table S2 for ITO/AgNW/ITO composites with different thickness of ITO top layers. The sheet resistances were quite increased with the increase of ITO top layers' thickness. By combining those considerations, the ITO overcoat layer on AgNWs should be controlled as thin as possible, as long as the conformal overcoat-layer is well-formed.

The ZnO layer on the ITO/AgNW/ITO composite was also fabricated by the combustion sol-gel method, and served as a hole blocking layer as well as an additional halogen ion barrier for AgNWs. Scanning electron microscope (SEM) images of ITO/AgNW/ITO and ZnO/ITO/AgNW/ITO composite

Nanoscale Accepted Manuscript

electrodes demonstrated thorough coating of a thin ITO layer on top of the AgNWs (Fig. 4b). By taking back-scattered electron (BSE) COMPO mode SEM images, we confirmed that the network of AgNWs was maintained even after annealing of solution-derived ITO and/or ZnO layers. We next measured the optical transmittance of the composite electrodes, including the ZnO layer (Fig. 4c). The transmittance (*T*) values at 550 nm were ~80%, and slight differences were observed depending on the AgNW density. Commercial FTO glass had a *T* of 81% at 550 nm. The inset photograph shows the visual transparency of the ZnO/ITO/AgNW(CAR=27%)/ITO composite on glass substrate. XRD analysis was also performed on the resulting ZnO/ITO/AgNW/ITO composite electrode to verify the effect of composite structure to prohibit the AgI formation. As shown in Fig. S6†, ESI, no apparent AgI peaks were observed for PbI_2/ZnO/ITO /AgNW/ITO sample even after aging for 24 hours.

To confirm the feasibility of using solution-processed ZnO/ITO/AgNW/ITO composite electrodes in perovskite solar cells, we fabricated $CH_3NH_3PbI_3$-based perovskite solar cells through a sequential deposition method[4] with the aid of a mesoporous Al_2O_3 (m-Al_2O_3) scaffold to allow for a sufficiently thick $CH_3NH_3PbI_3$ layer. We could not use a mesoporous TiO_2 (m-TiO_2) layer in our device architecture, because AgNWs are unable to withstand the high annealing temperature (~500°C) at which TiO_2 mesoporous layers are typically produced. Instead of m-TiO_2, we used m-Al_2O_3 as a scaffold layer as the latter can be prepared at a temperature as low as 200°C.[20] m-Al_2O_3 scaffolds have been widely used in mixed perovskite ($CH_3NH_3PbCl_xI_{3-x}$) solar cells, and it allowed us to improve the current density (J_{SC}) by forming a sufficiently thick $CH_3NH_3PbI_3$ absorber layer. Fig. 5a shows the influence of m-Al_2O_3 scaffold on top of the compact TiO_2 in terms of the perovskite absorber thickness. The AgNWs were well maintained after deposition of both m-Al_2O_3 and perovskite layers. As the presence of m-Al_2O_3 scaffold allowed for the increased perovskite layer, the current density was dramatically enhanced as shown in Fig. 5b.

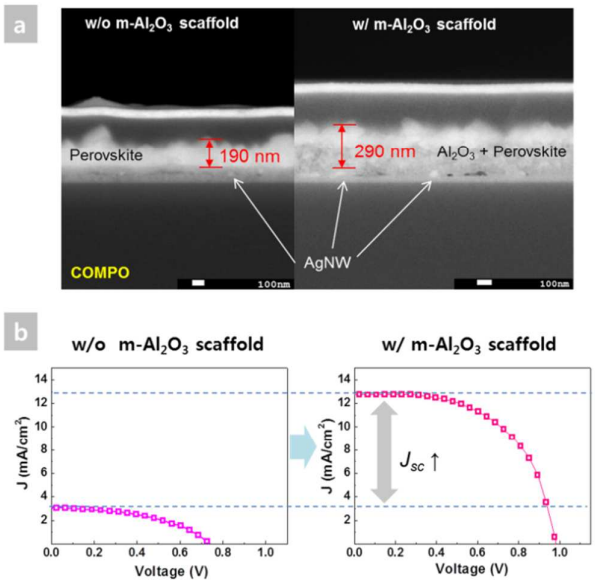

Fig. 5 (a) Cross-sectional SEM images of devices with and without a mesoporous Al_2O_3 (m-Al_2O_3) scaffold layer. (b) The current density-voltage (*J-V*) characteristics of the devices with and without m-Al_2O_3. J_{SC} was enhanced by introducing a m-Al_2O_3 scaffold layer

Microstructural morphologies of perovskite films prepared on different substrates are shown in Fig. S7†, ESI. The ZnO/ITO overcoat layer on top of the AgNW-networked web enabled deposition of uniform perovskite film without deformation of the AgNWs themselves by effectively suppressing the side-reactions of both AgI formation and Ag-phase corrosion. A thicker, uniform perovskite layer was obtainable with the m-Al_2O_3 scaffold framework. The cross-sectional structure of the resulting device is displayed in Fig. 6a. The FE-SEM image taken in COMPO mode distinguished each constituent layer: (i) AgNWs were sandwiched between oxide layers and maintained their original characteristic morphology and (ii) the ZnO/ITO/AgNW/ITO composite layer had an overall thickness of ~120 nm, which is thinner than the thickness of typical FTO substrates (~450 nm). To compare the ITO/AgNW/ITO composite electrode with a sputtered FTO electrode, all component layers other than the bottom electrode were fabricated identically. *J-V* curves are plotted in Fig. 6b and electrical parameters are listed in Table 1. Hysteresis and external quantum efficiency (EQE) data are plotted in Fig. S8† and S9†, ESI.

A reference cell using the FTO glass substrate (TEC-15, Pilkington),Au/Spiro-OMeTAD/$CH_3NH_3PbI_3$/m-Al_2O_3/ZnO/FTO, had a power conversion efficiency (PCE) of 10.81%. The device employing the AgNW-based composite electrode, Au/Spiro-OMeTAD/$CH_3NH_3PbI_3$/m-Al_2O_3/ZnO/ITO/AgNW/ITO, had a PCE of 8.44%. The efficiency of the cell with the AgNW-based composite electrode was slightly lower than that of the FTO cell. Nevertheless, this is the first demonstration of an all solution-processed, AgNW-based bottom transparent electrode, and the data indicate that this electrode can feasibly be used in perovskite solar cells. We attributed the slightly lower performance, especially with regard to short circuit current density (J_{SC}), to the lower transmittance and higher sheet resistance of the composite electrode. The average transmittance in the wavelength of 350–800 nm and sheet resistance were 72.5% and 18 ohm/sq for the ITO/AgNW(CAR = 31%)/ITO/glass substrate, and 78.8% and 15 ohm/sq for the FTO/glass substrate, respectively. The optical/electrical properties of the composite electrode can potentially be improved by optimizing the optoelectrical properties of the oxides, the density of AgNWs, and/or the thickness of each component layer. These changes could potentially enhance device performance to the extent that the PCE would exceed 10%.

The best performing device was achieved with an AgNW areal density condition of CAR=31%. By comparing the efficiency distribution for 27 devices with different CAR values, we observed that the average value of the overall data moved toward a higher efficiency region as the CAR

Nanoscale Accepted Manuscript

This journal is © The Royal Society of Chemistry 20xx

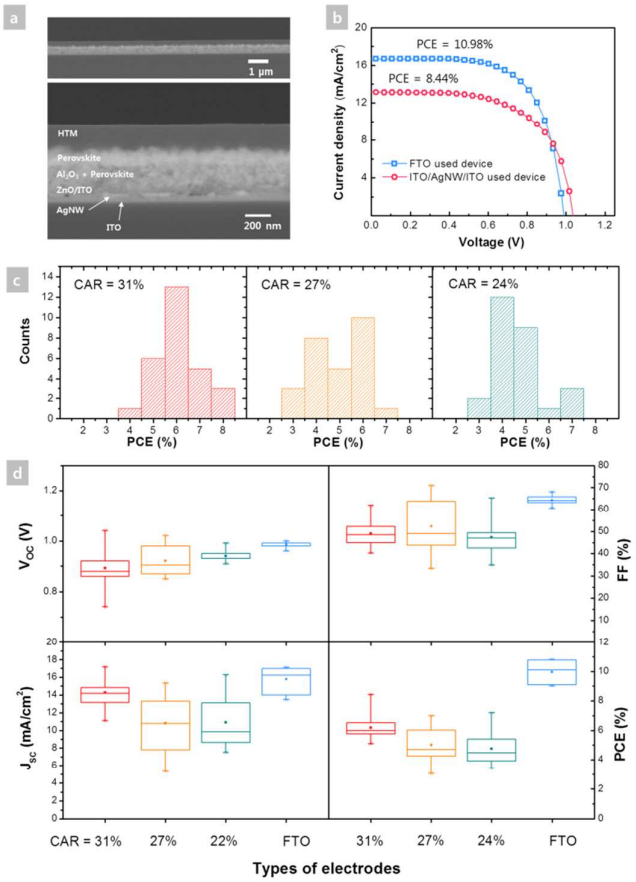

Fig. 6 (a) Cross-sectional FE-SEM image of Spiro-OMeTAD/$CH_3NH_3PbI_3$/m-Al_2O_3/ZnO/ITO/AgNW/ITO in BSE COMPO mode. (b) Current density-voltage (J-V) curves of the devices: (□) Au/Spiro-OMeTAD/ $CH_3NH_3PbI_3$/m-Al_2O_3/ZnO/FTO and (○) Au/Spiro-OMeTAD/$CH_3NH_3PbI_3$/m-Al_2O_3/ZnO/ITO/AgNW/ITO under standard 1 sun AM 1.5 G simulated solar irradiation. (c) Histogram of solar cell efficiencies according to the density of AgNWs in the composite electrodes. (d) Device performance statistics of V_{OC}, J_{SC}, FF, and PCE as a function of electrodes type. The three horizontal lines in the box indicate the 25th, 50th and 75th percentiles of the devices. The squares (■) represent the average values and the crosses (x) show the maximum and minimum values.

Table 1 Performances of the champion devices and average values fabricated for each condition under AM 1.5 illumination (100 mW cm^{-2})

Device type	V_{OC} [V]	J_{SC} [mA cm^{-2}]	FF [%]	PCE [%]
ITO/AgNW/ITO (CAR = 31%)	1.04	13.17	61.83	8.44
Average	0.89±0.07	13.91±2.2	48.52±5.3	6.12±0.8
ITO/AgNW/ITO (CAR = 27%)	1.02	12.57	54.43	6.99
Average	0.92±0.05	10.58±3.1	53.24±11.6	4.93±1.0
ITO/AgNW/ITO (CAR = 22%)	0.94	14.95	51.14	7.19
Average	0.94±2.9	10.73±2.9	47.66±8.1	4.68±1.1
FTO (TEC-15)	0.99	16.67	66.59	10.98
Average	0.99±0.01	15.78±1.4	64.30±2.1	9.97±0.7

value increased. This trend was closely associated with the density of the AgNW-networked web, as this web proportionally determines the conductivity of the AgNW-composite electrodes. However, AgNW film with a higher density has a lower optical transmittance and a rougher surface morphology. In particular, for multilayer-stacked composite electrodes, a rough AgNW-networked web surface adversely affects the formation of uniform protective oxide layers overlying the AgNW layer, which is of paramount importance for obtaining stable perovskite solar cells. As shown in Fig. 6d, the deviation in V_{OC} was wide for cells with a CAR value of 31%, and became narrower as the density of AgNWs decreased. However, the average values of J_{SC} and PCE were much higher for cells with a CAR value of 31% than those for cells with CAR values of 27 and 22%, as the resistance of AgNW-based composite film decreased as the density of AgNWs increased. This trend implied that the formation of a smoother surface in the sequentially-deposited, multi-layered composite electrodes was indispensible for achieving highly uniform performance and reproducibility. To further optimize AgNW-based composite electrodes, high conductivity and film uniformity are priorities. AgNWs appear to function as the main conduction path, and therefore have a significant effect on device performance. The role of AgNWs networks as a main conduction path can be clearly proved from the result of device without AgNWs, i.e. only sol-gel ITO electrode used device. As shown in Fig. S10†, ESI; device performances were quite lower than those of AgNWs used devices. This implies that the sol-gel based ITO electrode could not well operate as a highly conductive electrode, and the insertion of AgNWs can improve the conductivity of solution processed composite electrode. The bottom ITO layer also contributed to effective transportation of charge carriers through the empty areas between AgNWs, as shown in Fig. S11†, ESI; as the thickness of the bottom ITO layer increased from 40 to 80 nm, the J_{SC} improved from 8 to 14 mA cm^{-2}.

Together, our results indicate that composite electrodes comprising highly conductive, one-dimensional AgNWs structurally embedded inside a densely-formed, amorphous ITO matrix with a ZnO coating layer with hole blocking capability can function as an optoelectrically active layer through which light passes because of the optically transparent nature of the electrode and effective extraction of charge carriers to external circuits. Due to chemical degradation of the Ag phase by reaction with halogen ions in a time-dependent manner, we investigated the long-term stability of perovskite solar cells employing a AgNW-based composite electrode. Devices were evaluated as a function of storage time under ambient atmosphere (humidity of 30-48%, room temperature) after fabrication without encapsulation. As shown in Fig. 7, Efficiencies were well maintained until 14 days, followed by a slight decrement after 24 days. The exposure to humidity after device fabrication can be a main reason for this slight decrease of PCE, as when the AgI phase forms between electrode and perovskite layer, the device couldn't operate due to the conductivity loss in electrode and

Nanoscale Accepted Manuscript

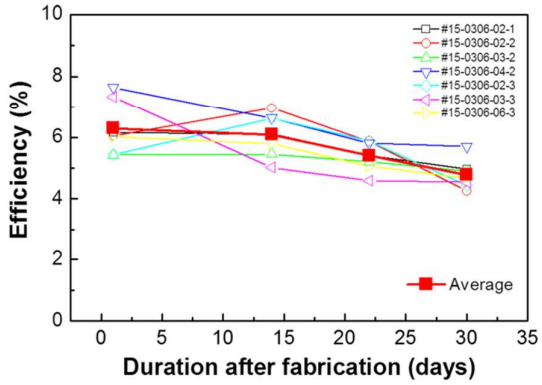

Fig. 7 Long-term stability test of the device with the configuration $CH_3NH_3PbI_3$/m-Al_2O_3/ZnO/ITO/AgNW/ITO. Power conversion efficiencies were measured as a function of duration after fabrication (1st day, 14th day, 24th day, and 30th day without encapsulation outside a glove box at a humidity of 30-48% and room temperature in air).

the phase deformation in perovskite layer. Therefore, this observation clearly demonstrates that a ZnO/ITO overlayer can stabilize AgNW-networked webs for a prolonged period of time by acting as a functional passivation layer.

Conclusions

In summary, this is the first demonstration of fully-solution-processed transparent conductive films for perovskite solar cells. Films were generated by introducing composite layers comprising Ag nanowires and low-temperature-processable, combustion sol-gel-derived metal oxide layers. To prevent chemical degradation of the Ag phase by reaction with highly reactive halogen ions from the perovskite precursor solutions, we designed multistacked ZnO/ITO composites that functioned as a transparent conductive layer, a chemical resistive layer, and a hole blocking layer. A $CH_3NH_3PbI_3$ solar cell employing the AgNW-based composite electrode had a PCE of 8.44%, the best value reported so far for perovskite solar cells fabricated with AgNW-based transparent electrodes. This demonstrates convincingly that perovskite absorbers ($CH_3NH_3PbI_3$, $CH_3NH_3PbCl_{3-x}I_x$, etc.) containing halogen ions can be deposited on AgNW-based electrodes. We are optimistic that further optimization of the configuration of composite electrodes will increase the PCE for perovskite solar cells based on the results reported in this study.

Acknowledgements

This research received financial support from a National Research Foundation of Korea (NRF) grant funded by the Korea government (MSIP) (No. 2012R1A3A2026417).

References

1 F. Guo, H. Azimi, Y. Hou, T. Przybilla, M. Hu, C. Bronnbauer, S. Langner, E. Spiecker, K. Forberich, C. J. Brabec, *Nanoscale* 2015, **7**, 1642.
2 H. Zhou, Q. Chen, G. Li, S. Luo, T. B. Song, H. S. Duan, Z. Hong, J. You, Y. Liu, Y. Yang, *Science* 2014, **345**, 542.
3 J. W. Lee, D. J. Seol, A. N. Cho, N. G. Park, *Adv. Mater.* 2014, **26**, 4991.
4 J. Burschka, N. Pellet, S.-J. Moon, R. Humphry-Baker, P. Gao, M. K. Nazeeruddin, M. Grätzel, *Nature* 2013, **499**, 316.
5 J. H. Im, I. H. Jang, N. Pellet, M. Gratzel, N. G. Park, *Nat. Nanotechnol. 2014,* **9**, 927.
6 Z. Ku, Y. Rong, M. Xu, T. Liu, H. Han, *Sci. Rep*. **2013**, *3*, 3132.
7 A. Mei, X. Li, L. Liu, Z. Ku, T. Liu, Y. Rong, M. Xu, M. Hu, J. Chen, Y. Yang, M. Grätzel, H. Han, *Science* **2014**, *345*, 295.
8 J. Krantz, T. Stubhan, M. Richter, S. Spallek, I. Litzov, G. J. Matt, E. Spiecker, C. J. Brabec, *Adv. Funct. Mater.* 2013, **23**, 1711.
9 C. H. Chung, T. B. Song, B. Bob, R. Zhu, H. S. Duan, Y. Yang, *Adv. Mater*. 2012, **24**, 5499.
10 B. E. Hardin, W. Gaynor, I. K. Ding, S.-B. Rim, P. Peumans, M. D. McGehee, *Org. Electron.* 2011, **12**, 875.
11 G. Y. Margulis, M. G. Christoforo, D. Lam, Z. M. Beiley, A. R. Bowring, C. D. Bailie, A. Salleo, M. D. McGehee, *Adv. Energy Mater.* 2013, **3**, 1657.
12 M. Song, D. S. You, K. Lim, S. Park, S. Jung, C. S. Kim, D.-H. Kim, D.-G. Kim, J.-K. Kim, J. Park, Y.-C. Kang, J. Heo, S.-H. Jin, J. H. Park, J.-W. Kang, *Adv. Funct. Mater*. 2013, **23**, 4177.
13 A. Kim, K. Woo, C.-H. Kim, J. Moon, *ACS nano* 2013, **7**, 1081.
14 A. Kim, Y. Won, K. Woo, S. Jeong, J. Moon, *Adv. Funct. Mater*. 2014, **24**, 2462.
15 D. Bryant, P. Greenwood, J. Troughton, M. Wijdekop, M. Carnie, M. Davies, K. Wojciechowski, H. J. Snaith, T. Watson, D. Worsley, *Adv. Mater*. 2014, **24**, 7499.
16 C. D. Bailie, M. G. Christoforo, J. P. Mailoa, A. R. Bowring, E. L. Unger, W. H. Nguyen, J. Burschka, N. Pellet, J. Z. Lee, M. Grätzel, R. Noufi, T. Buonassisi, A. Salleo, M. D. McGehee, *Energy Environ. Sci*. 2015, **8**, 956.
17 J. Han, S. Yuan, L. Liu, X. Qiu, H. Gong, X. Yang, C. Li, Y. Hao, B. Cao, *J. Mater. Chem. A* 2015, **3**, 5375.
18 M. G. Kim, M. G. Kanatzidis, A. Facchetti, T. J. Marks, *Nat. Mater.* 2011, **10**, 382.
19 S. D. Standridge, G. C. Schatz, J. T. Hupp, *Langmuir* 2009, **25**, 2596.
20 J. M. Ball, M. M. Lee, A. Hey, H. Snaith, *Energy Environ. Sci*. 2013, **6**, 1739.

Nanoscale Accepted Manuscript

This journal is © The Royal Society of Chemistry 20xx